Reaction Mechanisms

Deutsche Ausgabe: DOI: 10.1002/ange.201604388
Internationale Ausgabe: DOI: 10.1002/anie.201604388

Mechanistic Insights into Catalytic Ethanol Steam Reforming Using Isotope-Labeled Reactants

*Stephen Crowley and Marco J. Castaldi**

Abstract: *The low-temperature ethanol steam reforming (ESR) reaction mechanism over a supported Rh/Pt catalyst has been investigated using isotope-labeled EtOH and H_2O. Through strategic isotope labeling, all nonhydrogen atoms were distinct from one another, and allowed an unprecedented level of understanding of the dominant reaction pathways. All combinations of isotope- and non-isotope-labeled atoms were detected in the products, thus there are multiple pathways involved in H_2, CO, CO_2, CH_4, C_2H_4, and C_2H_6 product formation. Both the recombination of C species on the surface of the catalyst and preservation of the C–C bond within ethanol are responsible for C_2 product formation. Ethylene is not detected until conversion drops below 100 % at t = 1.25 h. Also, quantitatively, 57 % of the observed ethylene is formed directly through ethanol dehydration. Finally there is clear evidence to show that oxygen in the SiO_2-ZrO_2 support constitutes 10 % of the CO formed during the reaction.*

Precious metal nanoparticles dispersed on high-surface-area carriers have been demonstrated to exhibit superior capabilities in catalyzing chemical reactions.[1,2] Currently there is an interest in employing precious metal catalysts in oxygenated fuel reforming to produce hydrogen.[3–5] It is projected that the use of oxygenated feedstocks to produce chemicals will grow nearly fourfold from $3.6 billion in 2011 to $12.2 billion by 2021.[6] Ethanol is an excellent example of a platform feedstock targeted for reasons of current cost and availability.[7,8] However, the role of specific metals and supports in the reforming process is only well understood for oxygen-free hydrocarbon fuels. Base metals such as nickel and copper are ineffective at breaking the C–C bond within oxygenates and deactivate readily through coke formation.[9,10] Thus, precious metals are under investigation for the steam reforming process with bimetallic rhodium-based formulations showing increased activity and resistance to deactivation.[11–13] Despite their superior performance, there is still no consensus on how precious metals interact with reactant species to give rise to the products.

There are a myriad competing reactions contributing to the overall mechanistic understanding of ethanol steam reforming (ESR)[14] and they number in the hundreds.

[*] S. Crowley, Prof. Dr. M. J. Castaldi
Department of Chemical Engineering
City College of the City University of New York
New York, NY 10031 (USA)
E-mail: mcastaldi@ccny.cuny.edu

Supporting information and the ORCID identification numbers for the authors of this article can be found under: http://dx.doi.org/10.1002/anie.201604388.

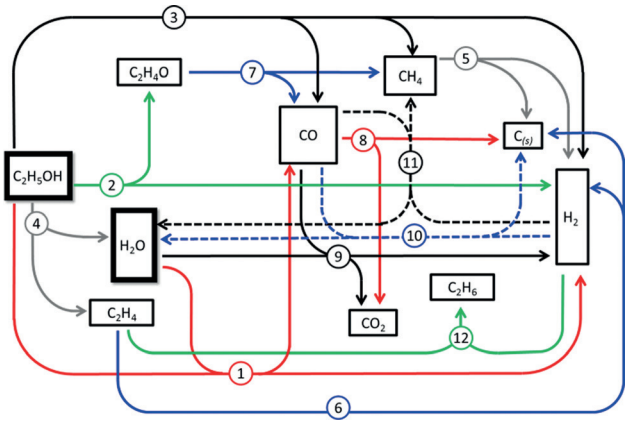

Figure 1. Possible reaction pathways during ethanol steam reforming. Circled numbers correlate to numbered Equations (1)–(12). Arrows represent forward reaction for simplicity.

Equations (1)–(12) and Figure 1 represent a fraction of what have been determined to be the dominant contributors.

$$\text{Steam Reforming}: \quad C_2H_5OH + H_2O \rightleftharpoons 2\,CO + 4\,H_2 \tag{1}$$

$$\text{Dehydrogenation}: \quad C_2H_5OH \rightleftharpoons C_2H_4O + H_2 \tag{2}$$

$$\text{Decomposition}: \quad C_2H_5OH \rightleftharpoons CH_4 + CO + H_2 \tag{3}$$

$$\text{Dehydration}: \quad C_2H_5OH \rightleftharpoons C_2H_4 + H_2O \tag{4}$$

$$\text{Methane Cracking}: \quad CH_4 \rightleftharpoons C + 2\,H_2 \tag{5}$$

$$\text{Ethylene Cracking}: \quad C_2H_4 \rightleftharpoons 2\,C + 2\,H_2 \tag{6}$$

$$\text{Acetaldehyde Decomposition}: \quad C_2H_4O \rightleftharpoons CH_4 + CO \tag{7}$$

$$\text{Boudouard Reaction}: \quad 2\,CO \rightleftharpoons C + CO_2 \tag{8}$$

$$\text{Water Gas Shift (WGS)}: \quad CO + H_2O \rightleftharpoons CO_2 + H_2 \tag{9}$$

$$\text{Reverse Carbon Gasification}: \quad CO + H_2 \rightleftharpoons C + H_2O \tag{10}$$

$$\text{Methanation}: \quad CO + 3\,H_2 \rightleftharpoons CH_4 + H_2O \tag{11}$$

$$\text{Ethylene Hydrogenation}: \quad C_2H_4 + H_2 \rightleftharpoons C_2H_6 \tag{12}$$

Classic reaction-model development focuses on measuring products over a range of test conditions combined with a proposed set of equilibrium reactions to match observed experimental data.[14–17] In a recent review on catalytic ESR by Hou et al., the authors highlight that there is no agreed upon reaction pathway for the overall ESR process.[14] Many researchers have contributed extensive experimental and

modeling efforts to elucidate the precise reaction sequence. Vesselli et al. utilize X-ray photoelectron spectroscopy (XPS) of adsorbed ethanol on a Rh(111) surface and UHV desorption experiments, while Resta et al. use density-functional theory (DFT) to determine major species formed during ethanol decomposition, thus showing experimentally and computationally that C–C bond cleavage is preferential to C–O bond scission.[18–21] In addition, the dehydrogenation reaction [Eq. (2)] on Rh/CeO_2 was studied by the group of Chen, thus showing that an oxametallacycle is formed with subsequent C–C bond cleavage and desorption to yield CH_4, H_2, and CO.[22] However, there is currently no consensus on the origin of the atoms constituting the final observed products for the steam reforming of higher-order hydrocarbons.

Isotope labeling is a longstanding technique used to gain insight into the likelihood of particular reaction pathways.[23–25] Song et al. used deuterated ethanol and water to determine the adsorption/desorption behavior of reactants,[26] as well as to investigate the reaction pathway of ethanol and water over CeO_2- and ZrO_2-supported cobalt.[27] Here we seek to provide new insights into a rhodium-based catalyst which dynamically changes oxidation states during reforming.[28] Through employing both isotope-labeled ethanol and water, it is now possible to track the atomic partitioning of the reactants into the products. Chemical formulas of the reactants, [1-^{13}C]ethanol and [^{18}O]water are shown in Figure 2.

In this study, isotope enrichment was 99% ^{13}C for [1-^{13}C]ethanol and 97.40% ^{18}O for [^{18}O]water (confirmed by GCMS). All non-H-atoms can be distinguished from one another, thus allowing for atom origin differentiation.

ESR was performed over 3 wt% Rh/1 wt% Pt, 4 wt% Rh, and 4 wt% Pt on SiO_2-ZrO_2 catalysts to determine the contribution of each metal to the overall product distribution. Bare SiO_2-ZrO_2 was found to be inactive in the process. All experiments were performed in a packed bed reactor at 350 °C and 1 atm. Other test parameters are available in the Supporting Information. The product distribution profile for the 3 wt% Rh/1 wt% Pt catalyst is shown in Figure 3 for the steam reforming of the isotope-labeled reactants. Product distribution profiles for the single-metal catalysts are available in the Supporting Information.

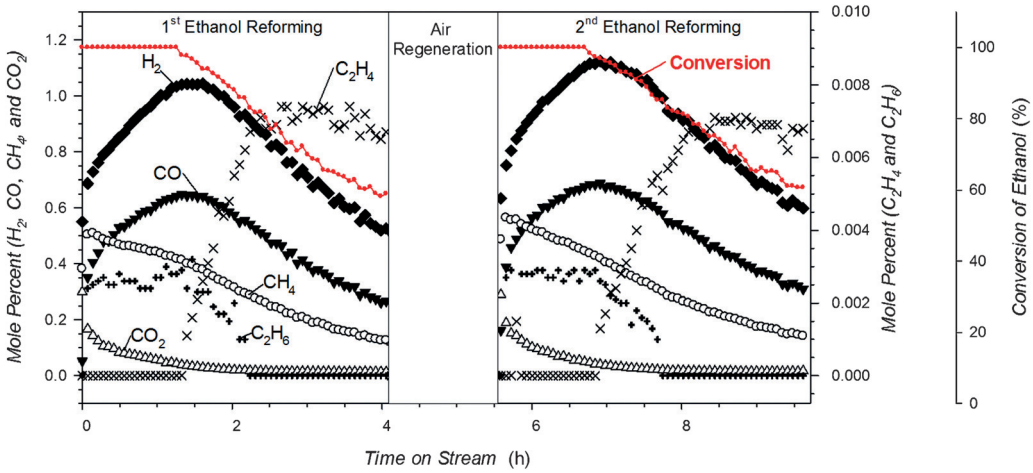

Figure 3. Product distribution profile for the reforming of [1-^{13}C]ethanol with [^{18}O]water over 3 wt% Rh/1 wt% Pt on SiO_2-ZrO_2 support. $T = 350$ °C, S/C = 1.5, GHSV = 44 000 h^{-1}.

The product distribution changed dynamically within the first four hours on stream, and is consistent with earlier work.[28] Evidenced in Figure 3, initially there was a steady increase in the amount of H_2, CO, and CH_4 produced, but CH_4 reached a maximum after 10 minutes then steadily decreased. The highest CO_2 production was observed at $t = 0$ and immediately decreased. C_2H_6 was produced at a near-constant rate during the first 1.25 hours on stream while no C_2H_4 was detected. At 1.25 hours, maxima were observed in H_2 and CO production followed by a steady decrease, thus indicating catalyst deactivation. This deactivation was further supported by ethanol conversion simultaneously falling below 100%. A selectivity change from C_2H_6 to C_2H_4 was also observed and it stabilized after 2.25 hours on stream with C_2H_4 concentrations of 0.007 mol% and no C_2H_6 detected. Identical features in the reforming product distribution profile are observed after a 1 hour regeneration in 5% O_2 in N_2. Only CO_2 (0.12 mole%) was detected during this time, thus suggesting oxidation of carbon deposited during reformation.

Interestingly, the single-metal catalyst formulations showed signs of deactivation after 0.5 hours on stream as opposed to 1.25 hours for the bimetallic catalyst (see Figures S1 and S2 in the Supporting Information). Overall, similar reforming behavior was observed between the 4 wt% Rh and 3 wt% Rh/1 wt% Pt formulations, and is not surprising given that they are both primarily rhodium-containing catalysts, with the bimetallic formulation providing the highest level of H_2 production at its maximum. However, the 4 wt% Pt catalyst exhibited a much lower

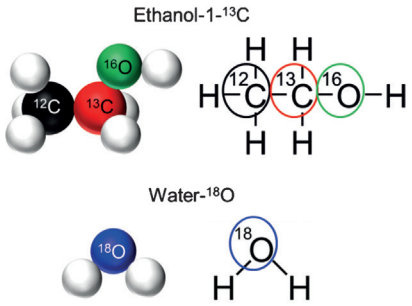

Figure 2. Isotope-labeled reactants [1-^{13}C]ethanol and [^{18}O]water.

selectivity for H_2 and increased selectivity for the C_2 species, thus suggesting platinum is less capable of breaking the C–C bond within ethanol.

Thus far we have shown what is commonly reported in the literature: the amount of each product detected as a function of time on stream. However, the origins of the atoms within each product are still unknown. Through examining the isotopic breakdown of individual species, we can now determine how the reactants partition into the products, thus giving us quantitative mechanistic insight.

The simplest isotope-labeled product differentiation occurs in CH_4. Two forms are possible, $^{12}CH_4$ and $^{13}CH_4$, and both were detected. Total mol% of CH_4 as a function of time on stream is presented in Figure 4 A, and a reproduction of the data presented in Figure 3 is shown with shaded areas representing each type of CH_4 detected. For the bimetallic catalyst, a maximum amount of $^{13}CH_4$ was detected initially at 0.18 mol% (33% of total CH_4), which decreased to 0.01 mol% after 2.25 hours. This outcome is surprising since $^{13}CH_4$ formation requires both the ^{12}C–^{13}C and the ^{13}C–^{16}O bonds in the ethanol to break. Similar behavior was observed for the 4% Rh catalyst formulation, though maximum $^{13}CH_4$ was detected at 10% of total CH_4 rather than 33%. 4 wt% Pt provided lower, near constant $^{13}CH_4$ at 2% of total methane.

From this data set, rhodium seems to be more capable of breaking the C–C bond in ethanol with either the ^{12}C–^{13}C bond breakage rate decreasing with time on stream or remaining constant while selectivity toward other ^{13}C-containing products increases, thus accounting for the decrease in observed $^{13}CH_4$. However the monotonic decline in the CH_4 for all catalyst formulations suggests the ^{12}C–^{13}C bond scission becomes less favored since the concentration profiles change more abruptly for other ^{13}C products. This observation will be discussed further with respect to the C_2 species. Similar tracking was performed for the C_2H_x and CO_y products (Figures 4 B–E).

The C_2H_6 formed (Figure 4 B) is initially observed to have a composition of 65% $H_3{}^{12}C{}^{12}CH_3$, and it decreases to 55% of total C_2H_6 produced over the first 2 hours of ESR. Since the two ^{12}C atoms must come from separate [1-^{13}C]ethanol molecules, this shows that the C_2H_6 formation pathway occurs primarily by breaking the ^{12}C–^{13}C bond within [1-^{13}C]ethanol and recombination with another ^{12}C species, and is consistent with the formation of $^{13}CH_4$. Similar behavior is observed for the rhodium-only formulation.

As discussed by Vesselli et al., it is likely that the ^{12}C–^{13}C bond within [1-^{13}C]ethanol is cleaved prior to recombination with a separate ^{12}C species.[18] Following this logic, it seems that the abundance of $H_3{}^{13}C{}^{12}CH_3$ at levels of 35–45% can be attributed to, first, a breaking of the ^{12}C–^{13}C bond within [1-^{13}C]ethanol and subsequent breaking of the ^{13}C–^{16}O bond, thereby allowing the ^{12}C and the ^{13}C moieties to recombine into ethane. This theory is supported by the presence of

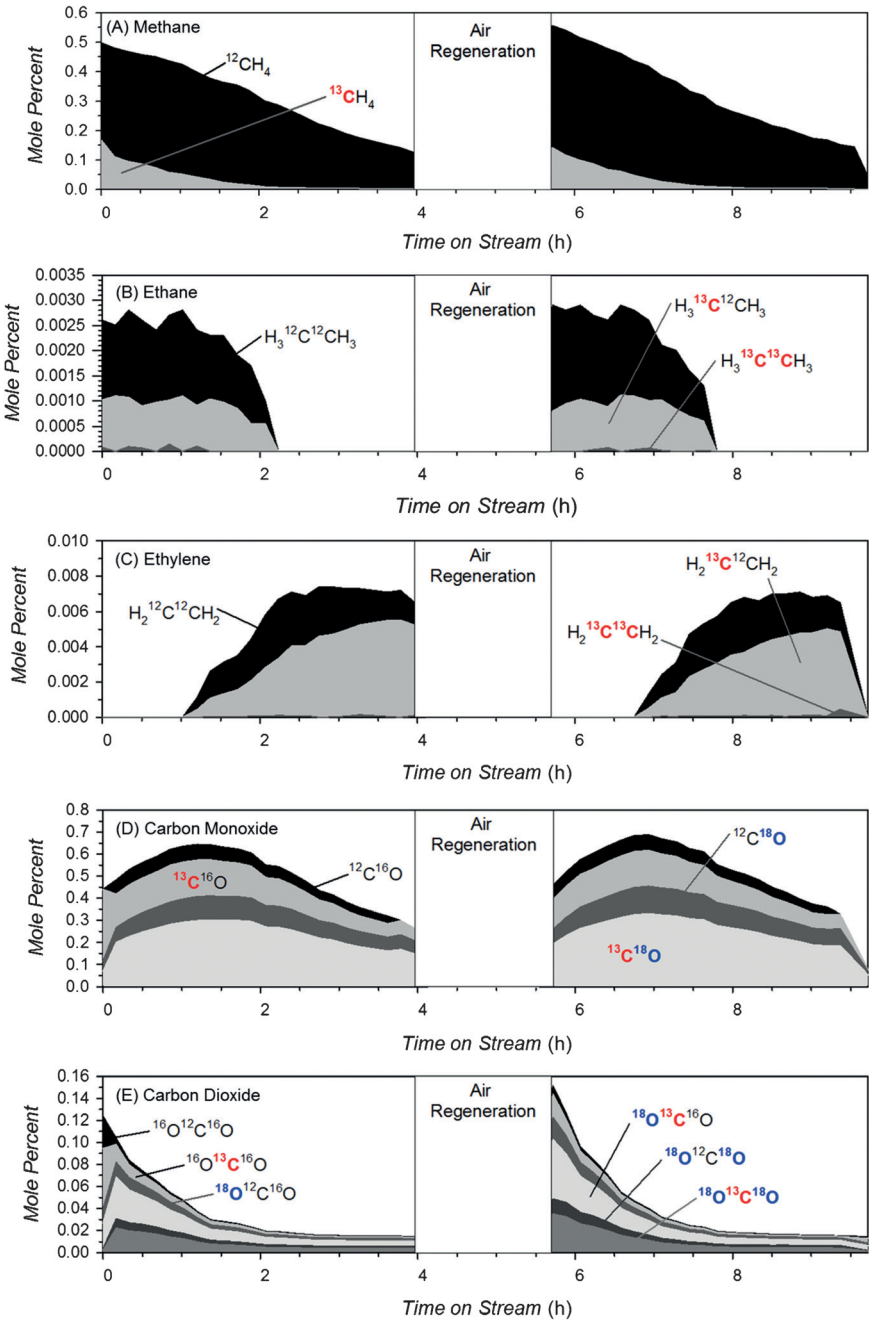

Figure 4. Atomic partitioning of ^{12}C,^{13}C, ^{16}O, and ^{18}O into A) methane, B) ethane, C) ethylene, D) carbon monoxide, and E) carbon dioxide over 3 wt% Rh/1 wt% Pt on SiO_2-ZrO_2. Bold colored text indicates isotope labeling.

$H_3{}^{13}C^{13}CH_3$. Even though this form of C_2H_6 is detected at low levels, the only way for this molecule to form is through breaking the $^{13}C–^{16}O$ and the $^{12}C–^{13}C$ bonds in ethanol, thus allowing two ^{13}C species to recombine into ethane. On the contrary, the platinum-only catalyst formulation yields ethane with $H_3{}^{13}C^{12}CH_3$ making up 95% of the total, thus further demonstrating that platinum is ineffective at breaking the C–C bond within ethanol. For all catalyst formulations, however, much of the ^{13}C goes to the CO_y species, thus maintaining a low concentration of $H_3{}^{13}C^{13}CH_3$.

A similar explanation can be applied to C_2H_4 (Figure 4C) with similar trends observed across the three catalyst formulations. C_2H_4 and C_2H_6 formation have a strong correlation since the formation of C_2H_6 (all isotopes) declines and C_2H_4 concentration increases concurrently. This selectivity change suggests that a portion of the C_2H_4 is formed directly from the C_2H_6 by the gas-phase dehydrogenation pathway.[29,30] However, this reaction is unfavored at the operating temperature of 350 °C,[31] thus implying that the C_2H_6 observed must be formed through ethylene hydrogenation [Eq. (12)] on the catalyst surface, a commonly reported feature of supported platinum-group metal catalysts.[32–34] We hypothesize that the tradeoff between C_2H_6 and C_2H_4 production observed at $t = 1.25$ h implies that the ethylene hydrogenation reaction is suppressed as the catalyst deactivates, and it is consistent with the emergence of ethylene as a stable product and the simultaneous decreases in H_2 and ethanol conversion.

However, the amount of C_2H_4 observed cannot be solely attributed to the prevention of the hydrogenation reaction. Stable C_2H_4 production was observed at 0.007 mol%. Since stable C_2H_6 production was observed at 0.003 mol%, this leaves 0.004 mol% (57%) of C_2H_4 unaccounted for. By examining the corresponding isotope-labeled components of C_2H_6 and C_2H_4, insight can be gained into the most likely ethylene production pathway. The amount of both $^{12}C–^{12}C$ and $^{13}C–^{13}C$ ethane and ethylene observed before and after the tradeoff in selectivity at $t = 1.25$ h indicates that the ethylene hydrogenation reaction is blocked for ethylene formed from identical carbon atoms. The $^{12}C–^{13}C$ ethane and ethylene, however, are a different matter. $H_3{}^{13}C^{12}CH_3$ is observed at 0.001 mol% during stable C_2H_6 production whereas $H_2{}^{13}C^{12}CH_2$ is observed at 0.005 mol% during stable C_2H_4 production. Thus, the 0.004 mol% of unaccounted-for C_2H_4 observed is entirely present as $H_2{}^{13}C^{12}CH_2$. Therefore, the decrease in $^{13}CH_4$ observed, as well as the minimal $H_2{}^{13}C^{13}CH_2$ detected, provide support for the ethanol dehydration pathway [Eq. (4)] as the most likely source of ethylene production.

The products become more complex for the CO_y species with two options for the carbon atom (^{12}C and ^{13}C) and two options for the oxygen atom(s) (^{16}O and ^{18}O). For the bimetallic and single-metal rhodium catalyst formulations, all four possible forms of CO (Figure 4D) are detected, thus proving that CO is not formed solely from the O-bound carbon atom within ethanol. Interestingly, for the rhodium-containing catalysts, $^{13}C^{18}O$ accounts for nearly 50% of the total CO detected throughout the test, and increases to 65% during the last 15 minutes of reforming. This occurrence is clear evidence that the primary pathway for CO formation is through direct reaction between the ethanol and water. Roughly 25% $^{13}C^{16}O$ was detected throughout the test, thus indicating that half as many $^{13}C–^{16}O$ bonds within [1-^{13}C]ethanol are preserved in CO formation. It can be seen that the ^{12}C entity recombines with ^{18}O from water to form $^{12}C^{18}O$, though only at 15% of total CO makeup. However, no $^{12}C^{16}O$ is detected at any point during reforming over the platinum-only catalyst. This result is expected since, upon first inspection, it would seem that the only source of ^{16}O is the carbon-bound oxygen atom in [1-^{13}C]ethanol. It would therefore be unlikely for the $^{13}C–^{16}O$ bond to break simply for the ^{16}O moiety to combine with a ^{12}C species on the catalyst, thus making it surprising to find that $^{12}C^{16}O$ is present throughout the reforming experiment for the rhodium-containing formulations. Thus, we propose that the CO formation pathway on rhodium-containing catalysts occurs not only through recombination of the ethanol and water reactants themselves, but also with the oxygen within the catalyst support as the only other source for ^{16}O.

Oxygen exchange between water and silica/zirconia supports has been well documented.[35–39] Tracking the composition of water in the effluent yielded a nearly constant isotopic concentration of 55% $H_2{}^{18}O$ and 45% $H_2{}^{16}O$. This outcome proves that $H_2{}^{16}O$ is formed consistently throughout the test, either through oxygen exchange with the support or through the dehydration, reverse carbon gasification, and methanation reactions [Eqs (4), (10), and (11) respectively]. In addition, the CO_2 concentration profile (Figure 4E) reveals that the WGS reaction [Eq. (9)] initially occurs, but gradually declines. Simultaneously, the CO concentration increases from 0.45 mol% at $t = 0$ to 0.65 mol% at $t = 1.25$ h, that is, more than the amount that can be provided by the decomposition of CO_2 (maximum observed concentration: 0.15 mole%) to CO. Consequently, the likely CO_y species which initially forms on the catalyst is CO, and it undergoes further oxidation to CO_2, supplied with oxygen from either the rhodium surface, the support itself, or water.

As evidenced, $^{12}C^{16}O$ is formed when the $^{12}C–^{13}C$ bond within [1-^{13}C]ethanol is broken, thus freeing a ^{12}C species which remains on the surface of the catalyst and allows reaction with ^{16}O on the support. This process is supported by a feature of the CO isotope product distribution occurring after 3.75 hours on stream. At this point, $^{12}C^{16}O$ is no longer observed in the products and suggests one of two phenomena: that the ^{16}O in the support near the metal–support interface has been completely depleted and replaced by ^{18}O from the labeled water, or that the bimetallic catalyst is no longer a pure alloy with platinum segregating to the surface and preventing recombination of the ^{12}C and ^{16}O species. Notably, $^{12}C^{16}O$ production resumes after the regeneration step and suggests that the oxygen in the support is replenished with ^{16}O, thus allowing the same phenomenon to occur in the second ethanol reforming ($t = 5.7$ h and later).

Interestingly, all six possible species of CO_2 are detected throughout the reforming experiments for the three catalyst formulations. While the amount of CO_2 decreased after an initial maximum, CO_2 showed the lowest variability in isotope product breakdown with nearly constant makeup as detailed

Table 1: Isotope product distribution for CO_2 during ethanol reforming.

CO_2 Isotope:	$^{16}O^{12}C^{16}O$	$^{16}O^{13}C^{16}O$	$^{18}O^{12}C^{16}O$	$^{18}O^{13}C^{16}O$	$^{18}O^{12}C^{18}O$	$^{18}O^{13}C^{18}O$
Composition:	4.3%	10.3%	14.3%	32.5%	12.3%	26.3%

in Table 1. Not surprisingly, the most abundant CO_2 isotope is $^{18}O^{13}C^{16}O$, in which the ^{13}C–^{16}O bond within [1-^{13}C]ethanol is maintained and combines with the ^{18}O from $H_2{}^{18}O$. However, the next most abundant species is $^{18}O^{13}C^{18}O$ where the ^{13}C–^{16}O bond is broken and the ^{13}C is bound to two ^{18}O centers. This step suggests that the second most likely process for CO_2 formation occurs by either the Boudouard reaction [Eq. (8)], where two $^{13}C^{18}O$ molecules react, or by the WGS reaction [Eq. (9)] where a $^{13}C^{18}O$ intermediate is formed and reacts with [^{18}O]water.

From our analysis, it is clear that the primary reaction pathways are changing as a function of time on stream. A figure has been included (Figure S5) and highlights the most likely dominant pathways at various stages of ESR. By using carefully selected isotope-labeled reactants, individual reaction pathways have been examined with an unprecedented level of clarity and trackability, thus allowing the unification of theory and experimentally observed results. The selectivity toward ethanol dehydration increased as the catalyst was deactivated. The presence of platinum within the catalyst makeup stabilizes rhodium performance and allows 100% conversion of ethanol for a time period nearly threefold that of the single-metal formulations. Rhodium is more effective at breaking the C–C bond within ethanol and allows more diverse species recombination than platinum. Support oxygen was shown to play a crucial role in the formation of reforming products, though platinum does not favor reaction between this oxygen and carbon species. The presence of all C and O isotopes within the products proves that bond preservation is not the only pathway for product formation. A recombination of species on the catalyst surface is occurring throughout the process for all catalyst formulations, thus indicating that a classic depiction of possible reactions [Eq. (1)–(12)] is incapable of completely describing species formation.

Acknowledgments

We thank Jeffrey LeBlanc and Prof. Dr. Ilona Kretzschmar for their feedback on the manuscript and Megan Webster, Robyn Smith, and the Combustion and Catalysis Laboratory for their support. We thank the Department of Chemical Engineering and the Earth Engineering Center at the City College of New York for their financial support under project number EEC | CCNY2012.

Keywords: heterogeneous catalysis · isotopic labeling · nanoparticles · reaction mechanisms · rhodium

How to cite: *Angew. Chem. Int. Ed.* **2016**, *55*, 10650–10655
Angew. Chem. **2016**, *128*, 10808–10813

[1] G. Bond, *Heterogeneous Catalysis*: *Principles and Applications*, Clarendon Press, Oxford, New York, **1987**.
[2] S. Duan, S. Senkan, *Ind. Eng. Chem. Res.* **2005**, *44*, 6381–6386.
[3] Q. Ming, *Catal. Today* **2002**, *77*, 51–64.
[4] M. Li, K. Duraiswamy, M. Knobbe, *Chem. Eng. Sci.* **2012**, *67*, 26–33.
[5] S. D. Angeli, G. Monteleone, A. Giaconia, A. A. Lemonidou, *Int. J. Hydrogen Energy* **2014**, *39*, 1979–1997.
[6] N. Deschamps, *The World Market for Bio-Based Chemicals*, 2nd ed., SBI Energy: EL Analysts, Rockville, MD, **2012**.
[7] P. B. Smith, G. F. Payne, *Renewable and Sustainable Polymers*, American Chemical Society, Washington, DC, **2011**.
[8] J. C. Serrano-Ruiz, R. Luque, A. Sepúlveda-Escribano, *Chem. Soc. Rev.* **2011**, *40*, 5266–5281.
[9] A. Carrero, J. A. Calles, A. J. Vizcaíno, *Chem. Eng. J.* **2010**, *163*, 395–402.
[10] J. Sehested, *Catal. Today* **2006**, *111*, 103–110.
[11] A. Bshish, Z. Yaakob, B. Narayanan, R. Ramakrishnan, A. Ebshish, *Chem. Pap.* **2011**, *65*, 251–266.
[12] M. A. Goula, S. K. Kontou, P. E. Tsiakaras, *Appl. Catal. B* **2004**, *49*, 135–144.
[13] F. Wang, W. Cai, C. Descorme, H. Provendier, W. Shen, C. Mirodatos, Y. Schuurman, *Int. J. Hydrogen Energy* **2014**, *39*, 18005–18015.
[14] T. Hou, S. Zhang, Y. Chen, D. Wang, W. Cai, *Renewable Sustainable Energy Rev.* **2015**, *44*, 132–148.
[15] M. Benito, J. L. Sanz, R. Isabel, R. Padilla, R. Arjona, L. Daza, *J. Power Sources* **2005**, *151*, 11–17.
[16] S. M. de Lima, A. M. Silva, U. M. Graham, G. Jacobs, B. H. Davis, L. V. Mattos, F. B. Noronha, *Appl. Catal. A* **2009**, *352*, 95–113.
[17] R. Trane-Restrup, S. Dahl, A. D. Jensen, *Int. J. Hydrogen Energy* **2013**, *38*, 15105–15118.
[18] E. Vesselli, A. Baraldi, G. Comelli, S. Lizzit, R. Rosei, *ChemPhysChem* **2004**, *5*, 1133–1140.
[19] A. Resta, J. Blomquist, J. Gustafson, H. Karhu, A. Mikkelsen, E. Lundgren, P. Uvdal, J. N. Andersen, *Surf. Sci.* **2006**, *600*, 5136–5141.
[20] E. Vesselli, G. Comelli, R. Rosei, S. Freni, F. Frusteri, S. Cavallaro, *Appl. Catal. A* **2005**, *281*, 139–147.
[21] A. Resta, J. Gustafson, R. Westerström, A. Mikkelsen, E. Lundgren, J. N. Andersen, M. M. Yang, X. F. Ma, X. H. Bao, W. X. Li, *Surf. Sci.* **2008**, *602*, 3057–3063.
[22] H.-L. Chen, S.-H. Liu, J.-J. Ho, *J. Phys. Chem. B* **2006**, *110*, 14816–14823.
[23] K. Otto, M. Shelef, J. T. Kummer, *J. Phys. Chem.* **1970**, *74*, 2690–2698.
[24] L. Shannon, J. G. Goodwin, *Chem. Rev.* **1995**, *95*, 677–695.
[25] R. M. Lum, J. K. Klingert, D. W. Kisker, S. M. Abys, F. A. Stevie, *J. Cryst. Growth* **1988**, *93*, 120–126.
[26] H. Song, X. Bao, C. M. Hadad, U. S. Ozkan, *Catal. Lett.* **2011**, *141*, 43–54.
[27] H. Song, L. Zhang, U. S. Ozkan, *Ind. Eng. Chem. Res.* **2010**, *49*, 8984–8989.
[28] S. Crowley, Y. Li, A. I. Frenkel, M. J. Castaldi, in *249th Am. Chem. Soc. Natl. Meet. Expo.*, Denver, CO, **2015**.
[29] F. E. Frey, D. F. Smith, *Ind. Eng. Chem.* **1928**, *20*, 948–951.
[30] F. O. Rice, R. E. Varnerin, *J. Am. Chem. Soc.* **1954**, *76*, 324–327.
[31] H. J. Dar, S. U. Nanot, K. J. Jens, H. A. Jakobsen, E. Tangstad, D. Chen, *Ind. Eng. Chem. Res.* **2012**, *51*, 10571–10585.
[32] Y. Okamoto, N. Ishida, T. Imanaka, S. Teranishi, *J. Catal.* **1979**, *58*, 82–94.

[33] S. Zhao, Y. Li, E. Stavitski, R. Tappero, S. Crowley, M. J. Castaldi, D. N. Zakharov, R. G. Nuzzo, A. I. Frenkel, E. A. Stach, *ChemCatChem* **2015**, *7*, 3683 – 3691.
[34] J. Grunes, J. Zhu, E. A. Anderson, G. A. Somorjai, *J. Phys. Chem. B* **2002**, *106*, 11463 – 11468.
[35] D. A. Hutchison, *J. Chem. Phys.* **1954**, *22*, 758.
[36] W. G. Spitzer, J. R. Ligenza, *J. Phys. Chem. Solids* **1961**, *17*, 196 – 202.
[37] B. W. Busch, W. H. Schulte, E. Garfunkel, T. Gustafsson, W. Qi, R. Nieh, J. Lee, *Phys. Rev. B* **2000**, *62*, 290 – 293.
[38] D. Martin, D. Duprez, *J. Phys. Chem.* **1996**, *100*, 9429 – 9438.
[39] J. Chelikowsky, D. Chadi, N. Binggeli, *Phys. Rev. B* **2000**, *62*, R2251 – R2254.

Received: May 5, 2016
Revised: July 12, 2016
Published online: August 3, 2016

